Investigation of Position Sensitive Avalanche Photodiodes for a New High Resolution PET Detector Design

Craig S. Levin, *Member, IEEE*, Angela M. K. Foudray, *Student Member, IEEE*, Peter D. Olcott, Frezghi Habte, *Member, IEEE*

***Abstract*-- We are developing a high resolution PET detector design with a goal of nearly complete scintillation light collection in ≤1 mm width, ≥ 20 mm effective thickness LSO crystals. The design uses position sensitive avalanche photodiodes in novel layered configurations that significantly improve the light collection aspect ratio. To reduce design complexity and dead area we are investigating the use of 1 mm thick sheets of LSO in addition to discrete crystal rods, and the use of PSAPDs which require only four readout channels per device. The raw spatial response of a 1 mm thick crystal sheet coupled to a PSAPD exhibits a compressed dynamic range compared to that observed with discrete crystals. Measurements with the proposed configurations using ^{22}Na irradiation achieved 10-13% FWHM energy resolution at 511 keV and 2 ns coincidence time resolution. 1 mm width crystals with a saw cut surface finish and no inter-crystal reflector were well resolved in flood images.**

I. Introduction

Recently there have been several groups developing high resolution Positron Emission Tomography (PET) systems dedicated to specific applications such as small laboratory animal and breast cancer imaging [1-10]. The standard approach to building high-resolution PET detectors uses an array of minute crystal rods with their narrow ends coupled to a photodetector array [1-10]. Extracting a significant fraction of the available light from the crystals in this manner proves to be difficult for ≤1 mm width crystal rods, especially since the rods should also be > 10 mm long for adequate coincident photon detection efficiency. Furthermore, cutting, finishing, and assembling minute crystal arrays is complex and costly.

We are developing a different high resolution PET detector design that promotes nearly complete scintillation light collection in ≤1 mm wide, ≥ 20 mm effective thickness lutetium oxyorthosilicate (LSO) crystals [11-12]. We are investigating novel layered configurations of avalanche photodiodes (APDs) that significantly improve the light collection aspect ratio compared to conventional designs for collection of nearly all available light created from a 511 keV interaction (*aspect ratio* is the ratio of crystal readout area to thickness; a higher ratio improves light collection efficiency).

We have previously studied linear APD arrays coupled to 1 mm thick LSO crystal sheets [12]. A drawback of APD arrays for a PET system is that the readout can be quite complex since each pixel requires its own low noise preamplifier and there are many pixels [12]. Thin crystal sheets compared to minute discrete crystals have the advantage that they are less complex to work with and have higher active crystal area, but the disadvantage that the light created from each scintillation event diffuses throughout the crystal. For discrete crystal array approaches we are investigating the conditions of no inter-crystal reflector and saw cut surface finish, which if successful, will greatly reduce crystal array manufacturing complexity.

To further reduce complexity for our high light collection concepts, this paper studies the use of position sensitive APDs (PSAPDs), which require only four readout channels per unit.

II. Materials and Methods

A. Scintillation Crystal Configurations

Figure 1 depicts the high light collection configurations we are investigating in this work, which comprise stacks of scintillation detector layers either edge-on or face-on with respect to incoming 511 keV photons. For high inter-*crystal* packing fraction, the two edge-on concepts shown in Figure 1 require very thin (<300 μm) PSAPDs that are currently under production. Although the two face-on designs do not require thin PSAPDs, for highest inter-*module* packing fraction they require PSAPDs with minimal surrounding dead area. The scintillation crystal material we have studied was LSO. 1 mm thick sheets of LSO have a very narrow light spread function which minimizes positioning non-linearities [11-12].

Manuscript received October 29, 2003. This work was supported by the National Institutes of Health under Grants No. EB 003283-01 from the National Institute of Biomedical Imaging and Bioengineering (NIBIB) and CA98691-01 from the National Cancer Institute (NCI), and Grant No. IMG00-000346 from the Susan G. Komen Breast Cancer Research Foundation.

C. S. Levin is with the VA Medical Center and the University of California San Diego (UCSD) School of Medicine, Department of Radiology, San Diego CA 92161 USA (telephone: 858-552-7511, e-mail: clevin@ucsd.edu).

A. M. Foudray, is with the UCSD Physics Department and the VA Medical Center, La Jolla, CA 92093 USA. (telephone: 858-5522-8585 x5364, e-mail: aklohs@physics.ucsd.edu).

P. D. Olcott is with the UCSD Computer Science Department and the VA Medical Center, La Jolla, CA 92093 USA. (telephone: 858-5522-8585 x5364, e-mail: aklohs@physics.ucsd.edu).

F. Habte is with the VA Medical Center and the UCSD School of Medicine, Department of Radiology, San Diego CA 92161 USA (telephone: 858-552-8585 x3594, e-mail: fhabte@ucsd.edu).

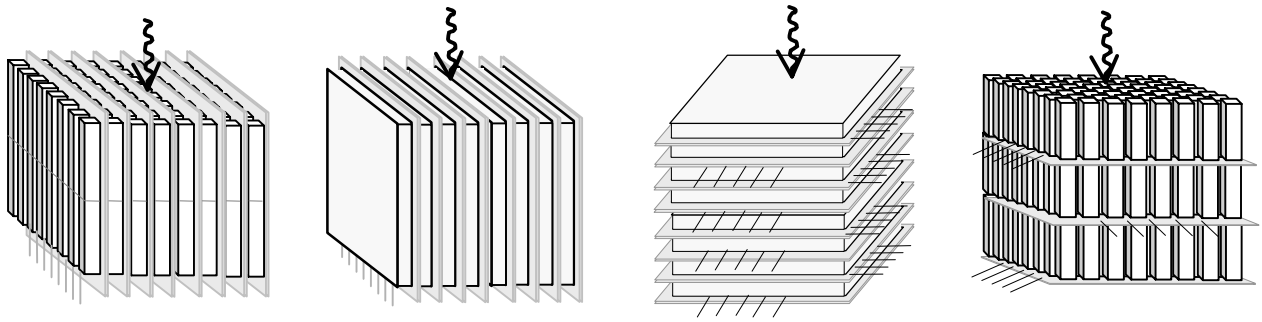

Fig. 1. Four scintillation detector configurations with very high light collection aspect ratio, each comprising layers of scintillation crystals coupled to position-sensing avalanche photodiodes (PSAPDs). Within any design the scintillation detector layers are each independent and comprise from left to right: Discrete crystal arrays or crystal sheets oriented "edge-on" with respect to incoming 511 keV photons; Stacked crystal sheets or short stacks of discrete crystal arrays oriented "face-on" with respect to incoming photons. All configurations shown can determine the interaction depth of the 511 keV photons.

Since each detector layer in each of these configurations is independent of the others, in this paper we study just one layer at a time as an indication of the performance of any given configuration. Positioning response of one detector array layer was measured using irradiation with a point ^{22}Na (511 keV) photon source. The crystal sheet layer we studied had dimensions of 8x8x1 or 8x8x2 mm^3 and was polished on all sides. The discrete crystal layers we studied were either 4x3 arrays of 2x2x3 mm^3 or 8x3 arrays of 1x1x3 mm^3 crystals that each had a ground "as cut" surface and no inter-crystal reflector. The outer area of the LSO in each layer (sheet or discrete array) was wrapped in 5 layers of Teflon tape.

B. Position Sensitive Avalanche Photodiode (PSAPD) Configurations

We used the high gain PSAPDs developed at Radiation Monitoring Devices (RMD), Inc. (Watertown, MA). The devices were fabricated using a planar process similar to that used for APD array fabrication [13]. The PSAPD devices we used had sensitive area of 8x8 and 14x14 mm^2, packaged on a ceramic substrate. In these devices four corner contacts are placed on the backside of the device which is covered by a high resistivity layer. The position of a light flash hitting the PSAPD front side is positioned using the four corner signals in an Anger-type logic. The energy and timing of each signal may be extracted from the common front surface contact or by summing the four back surface signals.

The operating gain of these devices is approximately 1000 at an operating bias of -1.766 V on the front surface contact, with the readout anodes at virtual ground. This operating bias provides the best 511 keV photopeak energy resolution in both devices. The PSAPD device capacitances are ~45 and 140 pf (0.7 pf/mm^2), the leakage current at operating bias is ~300-600 nA and 1-2 μA, and the rms noise is ~40 and 140 electrons, respectively, for the 8x8 and 14x14 mm^2 devices. The quantum efficiency of these devices are ≥60% for the 420 nm peak emission wavelength of LSO.

C. Measurements

We studied spatial and energy response of ^{22}Na 511 keV photon interactions in the LSO scintillation detector layers using both edge-on and face-on irradiation (see Figure 1). The four back side and common front side APD signals involved in each scintillation event are read out by discrete charge sensitive preamplifiers and NIM electronics, digitized, and sent to a Power Macintosh in list mode for post-processing. Each event was positioned with Anger-type logic. The coincidence time measurements were performed in a standard manner using a PMT coupled to a 6x6x8 mm^3 to provide the start signal for a time-to-amplitude converter (TAC) with the TAC stop determined from a 8x8x2 mm^3 LSO sheet coupled to the 8x8 or 14x14 mm^2 PSAPD.

III. RESULTS

A. Positioning Histograms for the Different Configurations

Figure 2 shows the 2-D positioning histogram from 511 keV flood irradiation of single scintillation detector layers from the two face-on designs of Fig. 1 comprising either a single crystal sheet or short discrete crystal array coupled to a PSAPD. The 8x8 mm^2 PSAPD was used for these measurements. Note that due to lateral light diffusion within the crystal sheet, the left flood image in Fig. 2 exhibits a reduced dynamic range compared to that for the discrete crystal array shown at the right. The measured energy spectrum for the sheet is inset.

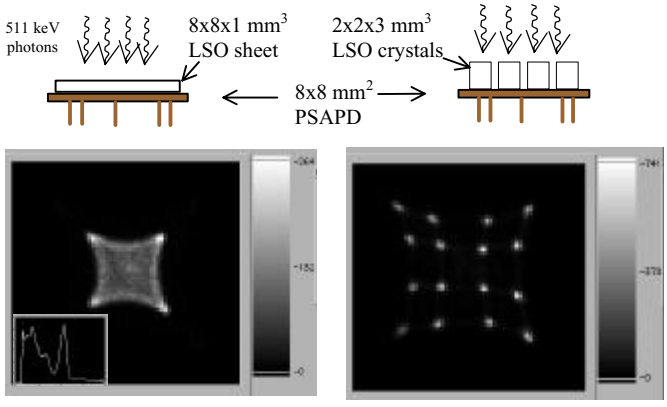

Fig. 2. 2-D histograms of positioned LSO scintillation detector events for one layer from each of the two face-on configurations depicted at the top, using an 8x8 mm^2 PSAPD. Left: Flood image for 1 mm thick crystal sheet. Inset: ^{22}Na energy spectrum with 12.3% FWHM energy resolution for the 511 keV photopeak. Right: Flood image for 4x4 array of 2x2x3 mm^3 crystals.

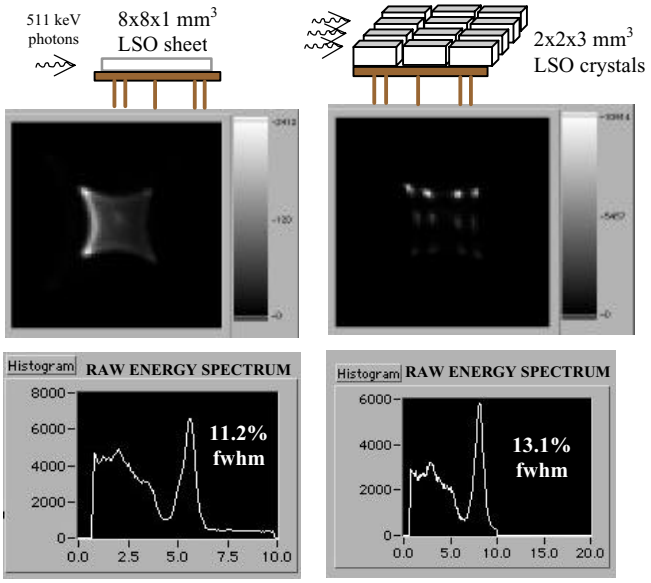

Fig. 3. 2-D histograms of positioned LSO scintillation detector events for one layer from each of the two edge-on irradiated configurations depicted at the top, using an 8x8 mm^2 PSAPD. Left: Image for 1 mm thick crystal sheet. Right: Image for 4x3 array of 2x2x3 mm^3 crystals coupled side-on to the PSAPD; this configuration facilitates a 3 mm interaction depth resolution. Below: Raw ^{22}Na sum energy spectra measured for these two cases.

Figure 3 shows the measured 2-D histograms and raw sum energy spectra for 511 keV interactions in both the crystal sheet and a discrete crystal array layer relevant to the edge-on irradiation concepts of Fig. 1. For the discrete array, the raw sum energy spectrum incorporates LSO crystal and PSAPD quantum efficiency variations across the detector layer into one spectrum. Thus, for discrete crystal arrays the most accurate technique to extract energy spectra and build calibration tables is through position-gating of individual crystals from the 2-D positioning histograms. As indicated in the top right of Fig. 3, this configuration facilitates a 3 mm interaction depth resolution.

B. Discrete Crystal Position-Gated Energy Spectra Comparisons for Side- and End-coupled Array Crystals

Figure 4 shows a comparison of crystal position-gated 511 keV photopeak pulse height and energy resolution extracted from the 2-D positioning histograms for the 4x3 array of 2x2x3 mm^3 LSO crystals coupled sideways to and the 4x4 array of the same crystals coupled end-on to the 8x8 mm^2 PSAPD. We see that even though the 2x2x3 mm^3 crystals are very short, since the light collection aspect ratio is considerably higher for the side-coupled case (3:1) compared to the end-coupled case (4:3) the individual crystal light pulse heights are larger and the variations in pulse height and energy resolution are smaller. The former case had an energy resolution range from 9.9-11.0% FWHM (average: 10.4%) over the 12 side-coupled array crystals, while that for the latter was 9.9-13% FWHM (average: 11.2%) for the 16 end-coupled crystals. Also shown is the position-gated energy spectrum with the best photopeak resolution (9.94% FWHM).

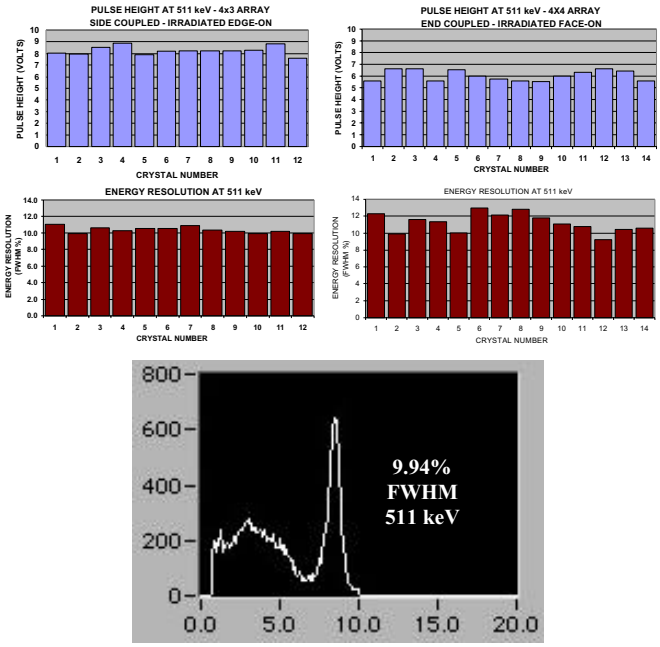

Fig. 4. Comparison between 511 keV photopeak pulse height (top plots) and energy resolution (middle plots) for individual 2x2x3 mm^3 LSO array crystals coupled sideways (left) and end-on (right) to an 8x8 mm^2 PSAPD. Bottom: Best single crystal energy spectrum for the side-coupled array.

C. Energy Resolution Comparison Between 8x8 and 14x14 mm^2 PSAPD Devices

Figure 5 shows a comparison between measured photopeak energy resolutions for the individual crystals of the 4x3 array of 2x2x3 mm^2 LSO crystals side-coupled to the 8x8 or 14x14 mm^2 PSAPD. Because the larger area device has higher bulk leakage current and capacitance, the device dark noise and crystal energy resolutions are systematically worse.

D. Discrete Crystal Identification Comparison for 8x8 and 14x14 mm^2 PSAPD Devices

Figure 6 shows ^{22}Na flood irradiation positioning histograms for the 4x3 array of 2x2x3 mm^3 LSO crystals coupled sideways to the 8x8 and 14x14 mm^2 PSAPDs. Also shown is the 1-D profile histogram through one of the crystal rows. Because the larger area device has higher bulk leakage current and capacitance, the crystal peak to valley ratios are systematically worse and the crystals are not as clearly distinguished.

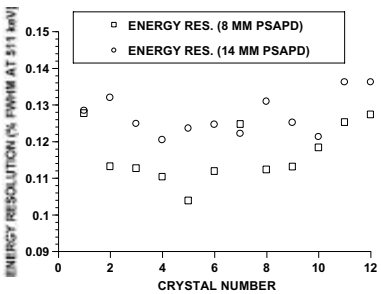

Fig. 5. Plot of 511 keV photopeak energy resolution for individual crystals of a 4x3 array of 2x2x3 mm^3 LSO crystals side-coupled to 8x8 and 14x14 mm^2 PSAPDs (similar to that depicted in Fig. 2, top right).

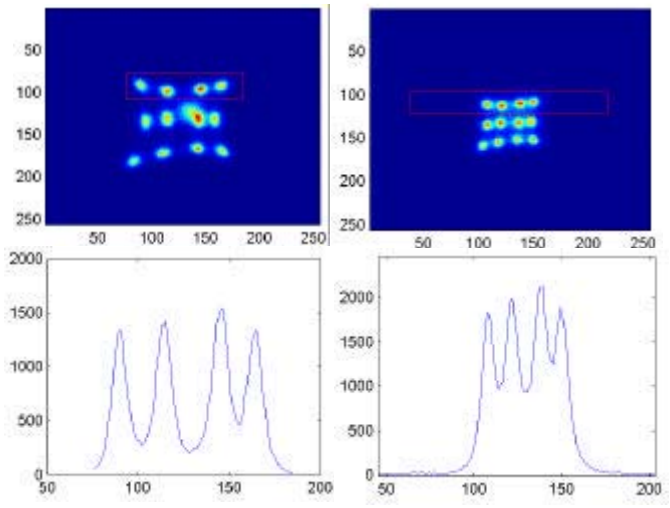

Fig. 6. Top: 2-D ^{22}Na flood histograms of the 4x3 array of 2x2x3 mm^3 LSO crystals side-coupled to the 8x8 (left) and 14x14 mm^2 (right) PSAPDs (similar to that depicted in Fig. 2, top right). Bottom: 1-D profile through top crystal rows of each flood image.

E. Coincidence Time Resolution Measurements with the 8x8 and 14x14 mm^2 PSAPD Devices

Figure 7 shows the measured TAC spectra for coincidences between the LSO-PMT and LSO-PSAPD channels. "Raw" TAC spectra data used a threshold just above the noise level in both the PMT and PSAPD. "Energy gated" TAC data used a 20% window about the 511 keV photopeak in each channel. The coincidence time resolution directly depends upon the fluctuation in the slope of the pulse rise in each channel. Since the 14x14 mm^2 PSAPD dark noise is worse and the capacitance is higher, the pulse rise variations are higher and the TAC spectra are broader (~3.3-3.4 ns FWHM) compared to that for the 8x8 mm^2 device (~2.0-2.8 ns FWHM).

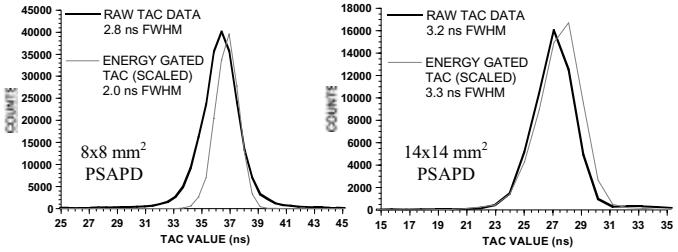

Fig. 7. Coincidence TAC spectra measured with (left) the 8x8 and (right) 14x14 mm^2 PSAPDs.

F. PSAPD Readout of 1 mm Crystal Array

Figure 8 shows results for an 8x3 array of 1x1x3 mm^3 LSO crystals side-coupled to the 8x8 mm^2 PSAPD, flood irradiated with a ^{22}Na source. In this measurement the top 9 crystals appearing in the flood image were saw cut on all faces, while the bottom 12 crystals were polished. The crystals were placed in the array without intercrystal reflector. The 1 mm array crystals were easily identified with peak/valley ratios ranging from 2-9. Three of the crystals were slightly off the edge of the sensitive area and recorded photopeak energy resolutions greater than 13.9% FWHM. The remaining crystals had 511

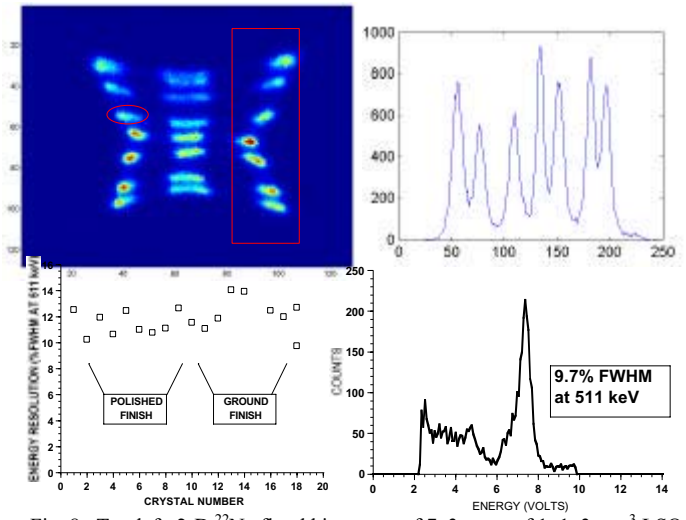

Fig. 8. Top left: 2-D ^{22}Na flood histogram of 7x3 array of 1x1x3 mm^3 LSO crystals side-coupled to the 8x8 mm^2 PSAPD (in a manner similar to that depicted in Fig. 2, top right). The surfaces of the top 9 crystals were saw cut, while those of the bottom 12 crystals were polished. No intercrystal reflector was used. Top right: Profile through one column of crystal array flood image indicates the excellent peak separation achieved for either surface condition. Bottom left: Plot of photopeak energy resolutions for the different array crystals. Bottom right: The best crystal energy spectra came from a saw-cut crystal indicated by a small ellipse in the flood image.

keV photopeak energy resolutions less than 13% FWHM. The best 1x1x3 mm^3 individual LSO crystal 511 keV photopeak energy resolution was 9.7% FWHM with saw-cut surfaces (see bottom right of Figure 8).

IV. Summary and Discussion

Our goal is to develop an ultra-high resolution detector with high detection efficiency, photon interaction depth resolution, and nearly complete collection of the available scintillation light from a 511 keV photon interaction. Optimizing light collection is important for high energy resolution. Excellent energy resolution allows one to use a narrow energy window about the photopeak, while still maintaining high count sensitivity. A narrow pulse height window reduces random and scatter background contamination and in doing so also helps to improve count rate performance.

The first three proposed configurations (Fig. 1) utilize layers of large area, position sensitive avalanche photodiodes that readout large faces of scintillation crystals for very high light collection aspect ratios. For these three configurations nearly all available light is collected, independent of the crystal geometry and surface finish. This property can be seen from the very similar energy resolutions measured from 2x2x3 and 1x1x3 mm^3 LSO crystals, for saw cut or polished surfaces (see Figs. 4 and 8). 1 mm discrete crystals are well resolved even with no inter-crystal reflector and saw cut finish. The fourth configuration in Fig. 1 utilizes short stacks of discrete crystals coupled end-on to the PSAPD. The light collection aspect ratio in this case is not as high as for the other three

configurations and, as a result, the pulse heights are smaller and both pulse height and energy resolution variations among crystals are larger (see Fig. 4). Thus we will no longer pursue that design. Edge-on orientations require very thin (<300 microns thick) APDs, which are currently being developed.

Use of crystal sheets instead of arrays of minute discrete crystals is desirable to reduce detector manufacturing complexity. However, due to light diffusion throughout the sheet crystal for every event, using Anger-type logic on the four corner signals for event positioning yields a compressed spatial dynamic range compared to the discrete crystal case (Fig. 2) since the maximum difference between signals along any given direction is reduced. Spatial compression also occurs for the side-coupled discrete crystal arrays (Figs. 3, 6 and 8) since there were no reflectors between crystals used in these studies and intercrystal light sharing occurred (although not as much for the 1x1x3 mm^3 crystal array; see Fig. 8). More intelligent positioning algorithms [14] are under investigation to expand the dynamic range of the sheet crystal imaging and improve linearity near the FOV edge.

The 8x8 and 14x14 mm^2 PSAPDs were compared in regards to 511 keV photopeak energy resolution, discrete crystal identification and coincidence time resolution for the same array of 2x2x3 mm^3 LSO crystals. In all cases the 8x8 mm^2 array performed systematically better than the larger PSAPD. The energy resolution ranged from ~10-13% FWHM in the former while that for the latter was ~12-14%. The crystal peak to valley ratios in the 2-D discrete crystal positioning histograms ranged from ~3-6 for the 8x8 mm^2 device, but only ~1.3-2 for the larger device. Finally, the coincidence time resolution measured using a 20% window about the photopeak in each channel was 2.0 ns FWHM in the 8x8 mm^2 device compared to 3.3 ns in the larger device. However, the 14x14 mm^2 device offers the distinct advantage of a factor of 3 larger sensitive area, which means a factor of 3 fewer devices and electronic channels are required for the same system scintillation crystal volume.

Achieving >20 mm effective LSO thickness for the edge-on configurations (Fig. 1, left two modules) would require roughly two and three stacks of those modules, respectively using the 14x14 and 8x8 mm^2 PSAPDs. The number of devices require to achieve the desired LSO depth for the third (face-on) design in Fig. 1 depends upon the crystal thickness utilized.

V. Conclusion and Future Directions

Our results indicate that PSAPDs can be used for high light collection configurations to optimize PET detector performance parameters such as energy, spatial and temporal resolutions. Presently we are taking steps to realize the detector modules depicted in Fig. 1. For the first two edge-on designs we are currently developing a <300μm thick PSAPD which will facilitate a 70% crystal packing fraction. Our experiments indicate that arrays of discrete saw cut crystals with no intercrystal reflector can be used, which reduces detector complexity and improves crystal packing fraction. For the sheet crystal designs we are investigating intelligent algorithms to improve the spatial dynamic range and linearity. To take full advantage of the high gain provided by the PSAPD we are developing compact, high input dynamic range, leakage current compensated front-end readout electronics.

VI. Acknowledgment

This work was supported by the National Institutes of Health under Grants No. EB 003283-01 from the National Institute of Biomedical Imaging and Bioengineering (NIBIB) and CA98691-01 from the National Cancer Institute (NCI), and Grant No. IMG00-000346 from the Susan G. Komen Breast Cancer Research Foundation. The authors would like to acknowledge Dick Farrel, Mickel McClish, Michael Squillante and Kanai Shah at RMD, Inc. for their ideas and support.

VII. References

[1] Miyaoka, R.S.; Kohlmyer, S.G.; Lewellen, T.K. Performance characteristics of micro crystal element (MiCE) detectors. *IEEE Trans Nucl Sci*, vol.48, (no.4, pt.2), Aug. 2001. p.1403-7.

[2] Y-C Tai, Chatziioannou, A.F., Dahlbom, M., Cherry, S.R. System design for a 1mm^3 resolution animal PET scanner: microPET II. *2000 IEEE Nuclear Science Symposium Conf. Rec*., vol.3, p.21/52.

[3] C.J. Marriott, J.E. Cadorette, R. Lecomte et. al. High Resolution PET Imaging and Quantitation of Pharmaceutical Biodistributions in a Small Animal Using APD Detectors. *J Nucl Med* 35:1390-7 (1994).

[4] C. Schmelz, SM Bradbury, I Holl, et al. 1995. Feasibility study of an avalanche photodiode readout for a high resolution PET with nsec time resolution. IEEE Trans.Nucl. Sci. 42:1080-4.

[5] Chatziioannou, AF, Cherry, SR, Shao, Y, et al. Performance Evaluation of microPET: A High-Resolution Lutetium Oxyorthosilicate PET Scanner for Animal Imaging. JNM, 40, 1164-1175, 1999.

[6] Jeavons, AP, Chandler, RA, Dettmar, CA. A 3D HIDAC-PET Camera with sub-millimetre resolution for imaging small animals. IEEE Trans Nucl Sci Vol 46 (No.3, Pt. 2), June 1999 (468-73).

[7] V.G. Zavarzin, H.A. Kudrolli, P.Y. Stepanov, I.N. Weinberg, L.P. Adler, and W.A.Worstell. First Results with PEM-X, a Compact Modular PET Breast Imager, IEEE Medical Imaging Conference Record (1999).

[8] Nan Zhang, Thompson CJ, Togane D, Cayouette F, Nguyen KQ. Anode position and last dynode timing circuits for dual-layer BGO scintillator with PS-PMT based modular PET detectors. IEEE Transactions on Nuclear Science, vol.49, no.5, pt.1, Oct. 2002, pp.2203-7.

[9] Smith MF, Majewski S, Weisenberger AG, Kieper DA, Raylman RR, Turkington TG. Analysis of factors affecting positron emission mammography (PEM) image formation. IEEE Transactions on Nuclear Science, vol.50, no.1, Feb. 2003, pp.53-9.

[10] Freifelder R, Cardi C, Grigoras I, Saffer JR, Karp JS. First results of a dedicated breast PET imager, BPET, using NaI(Tl) curve plate detectors. 2001 IEEE Nucl Sci Symp Conf Rec. Part vol.3, 2002, pp.1241-5 vol.3.

[11] C.S. Levin. Design of a High-Resolution and High-Sensitivity Scintillation Crystal Array for PET with Nearly Complete Light Collection. IEEE Trans Nucl Sci. Vol. 49, No. 5, October 2002.

[12] C.S. Levin and F. Habte. Initial Studies of a New Detector Design for Ultra-High Resolution Positron Emission Tomography. Conference Record of the 2002 IEEE Medical Imaging Conference. No. M11-150.

[13] Shah KS, Farrell R, Grazioso R, Myers R, Cirignano L. Large-area APDs and monolithic APD arrays. IEEE Transactions on Nuclear Science, vol.48, no.6, pt.2, Dec. 2001, pp.2352-6.

[14] Joung J, Miyaoka RS, Lewellen TK. cMiCE:a high resolution animal PET using continuous LSO with a statistics based positioning scheme. 2001 IEEE Nuclear Science Symposium Conference Record. 2002, pp.1137-41 vol.2.